Oxidation of Metals (2021) 95:85–104
https://doi.org/10.1007/s11085-020-10011-w

ORIGINAL PAPER

Stress Corrosion Testing of CMSX-4, CM247LC DS and IN6203DS Ni-Base Superalloys

Neil Chapman[1,2] · Simon Gray[2] · Joy Sumner[2] · John Nicholls[2]

Received: 20 October 2020 / Revised: 20 October 2020 / Accepted: 5 November 2020 /
Published online: 23 November 2020
© The Author(s) 2020

Abstract

The combination of stress and hot corrosion may result in Ni-base superalloys experiencing stress corrosion cracking, of which, the mechanisms are little understood. The aim of this research was to enhance the understanding by performing a series of stress corrosion exposures, at temperatures of 550, 500 and 450 °C, on: CMSX-4, CM247LC DS and IN6203DS superalloys. After completing the exposures, the superalloys were ranked with respect to the severity of the cracking experienced (CMSX-4 showing the worst severity, followed by CM247LC DS and then IN6203DS which showed no evidence of cracking at all) and the ranking appeared to be correlated to the gamma prime volume fraction. This suggests the gamma prime volume fraction is associated with the crack mechanism with lower values increasing the resistance to stress corrosion cracking. From the findings of this research, a new crack initiation/propagation mechanism is proposed which is based on a summation of stresses that includes those associated with the gamma prime.

Keywords Lattice mismatch · Interstitial atoms · Embrittlement

Introduction

Rotor blades are critical components of industrial gas turbines (IGT) which are subjected to high temperatures and stresses. This necessitates the use of materials for these components that have suitable high temperature mechanical properties, such as precipitation-hardened Ni-base superalloys. These materials have been developed over the years to optimise the mechanical properties [1], and this has enabled IGTs to operate at higher temperatures and efficiencies thus reducing the CO_2 emissions [2].

✉ Neil Chapman
chapman.neil@siemens.com

[1] Siemens Industrial Turbomachinery Ltd, Ruston House, PO Box 1, Waterside South, Lincoln LN5 7FD, UK

[2] Cranfield University, College Road, Cranfield, Wharley End, Bedfordshire MK43 0AL, UK

The precipitates, which have an ordered $L1_2$ fcc crystal structure [2], are Ni_3Al based particles (known as gamma prime) and may be strengthened by substituting the Al with other elements such as Ti, Ta and Nb [1]. The gamma prime precipitates are homogeneously dispersed and coherent within the disordered [3] fcc matrix (referred to as gamma) of the superalloy [2]. Due to a difference in the lattice constants between the gamma prime and gamma, a lattice mismatch (δ) exists at the interface between the two. Providing the lattice constants of the gamma prime ($a_{\gamma'}$) and gamma (a_{γ}) are known, the mismatch may be calculated using Eq. 1 [3–6]:

$$\delta = \frac{2\left(a_{\gamma'} - a_{\gamma}\right)}{a_{\gamma'} + a_{\gamma}} \tag{1}$$

The lattice mismatch tends to be negative, with an approximate magnitude of 10^{-3}, at room temperature [6]. Owing to a difference in the thermal expansion properties between the two phases, the magnitude of the lattice mismatch increases with increasing temperature [6]. At temperatures between 400 and 650 °C, the gamma begins to experience a greater increase in the lattice constant than that of the gamma prime [4] creating high stresses at the interface [7]. These stresses may be relieved at higher temperatures as the gamma prime starts to raft and a network of edge dislocations, slipping from the gamma, begin to form at the interfaces [7]. These networks may be either beneficial or detrimental (depending on the material, stress and temperature conditions) to the creep properties. That is, the dislocation networks may either act as a barrier to dislocation movement or as a source of dislocations into the gamma prime [7]. During thermal and mechanical loading, the ordered structure of the gamma prime tends to hamper dislocations moving from their source, but once a dislocation has entered the gamma prime, the ordered structure is disrupted, and an antiphase boundary created. The ordered structure may be restored if a second dislocation enters the gamma prime on the same slip plane. The pairing of dislocations then restricts further dislocation movement into the gamma prime resulting in improved creep properties [2]. Development of the superalloys has seen some modern versions with gamma prime volume fractions up to 70% [2, 4, 6] thus optimising the creep properties and increasing the hardness [2]. This has been achieved by increasing the proportion of elements, such as Ni, Al, Ta and Ti, within the chemistry of the superalloy which enrich the gamma prime [4]. Conversely, reducing these proportions and increasing the proportion of elements which enrich the matrix, such as Cr and Co [4], decreases the gamma prime volume fraction.

Adding Al and Cr to the chemistries of the Ni-base superalloys also has another effect: the ability to grow a protective scale of either alumina or chromia. These slow growing scales initially form alongside transient oxides, such as NiO and CoO, until the protective scales have formed a continuous layer. At this point, the transient oxides stop growing since a barrier has been created which stops the oxygen reacting with the respective elements within the chemistry, thus improving the oxidation resistance of the superalloy [8].

The protective scales also offer a degree of resistance to hot corrosion, which requires the presence of deposits such as Na_2SO_4 to induce the attack [8, 9]. At temperatures around 900 °C, these deposits are in a melted form and Type I hot

corrosion occurs. At temperatures around 700 °C the deposits are in a solid state and, providing SO_3 is present in the gas stream, may interact with transient oxides to form a melted sulphate system which initiates Type II hot corrosion [8, 9]. Both Type I and II hot corrosion attack any protective scale present by dissolving it into the melted sulphates [10]. The protective scale may repair itself by selective oxidation [10] of the element responsible for the scale (Al or Cr) from the chemistry of the superalloy [11]. During this period, known as incubation, the rate of attack is low. Once the responsible element has been consumed from the chemistry, the protective scale can no longer be repaired, at which point the attack enters a propagation stage and accelerated attack of the superalloy is experienced [8, 9, 11]. Hot corrosion may also occur with the deposits remaining in the solid state [12–14]. One example of this form of hot corrosion was provided by Kistler et al. [15] after hot corrosion exposures were performed at 550 °C on a Ni-base superalloy using Na_2SO_4 deposits and a gaseous environment of SO_2 in O_2. It was proposed that the deposits had reacted with Ni diffusing through the transient oxide NiO to form a metastable nanocrystalline mixed oxide ($Na_2Ni_2SO_5$) which allowed rapid Ni fluxing. It was also suggested a similar reaction may occur with Co to produce another metastable nanocrystalline mixed oxide ($Na_2Co_2SO_5$) and further accelerate the attack.

The temperature at which the mixed oxides formed (550 °C) coincides with the temperature range which start to cause increased magnitudes of the lattice mismatch (400 to 650 °C). This suggests that the interface between the gamma prime and gamma is not only at risk from hot corrosion attack but also from stress corrosion cracking especially if an additional stress is applied. Computer modelling of a simple Ni-base superalloy using Ni, Al, Re and S atoms, by Chen et al. [16], indicated a gamma prime susceptibility to embrittlement. The modelling showed that Ni and Al atoms adjacent to the interface could form strong covalent bonds with interstitial S atoms through the accumulation of significant quantities of electrons. The Ni-S bonds were adjacent to the interface within the gamma region whilst the Al-S bonds were normal to the interface within the gamma prime. The formation of the strong Ni-S and Al-S bonds came at the expense of the Ni–Ni and Ni–Al bonds which became weaker due to electron depletion for these bonds and hence created an embrittlement. Brooking et al. [17] demonstrated the risk of stress corrosion cracking by performing a series of 550 °C hot corrosion tests on CMSX-4. It was suggested that a combined hot corrosion stress mechanism initially attacked the gamma prime after which cracks propagated through the precipitates as the mechanism attacked the features ahead of the crack path.

Since the gamma prime appears to be highly susceptible to stress corrosion cracking, the aim of this research was to enhance the understanding and identify a property of the gamma prime which showed correlation. In addition, since temperature affects diffusion rates [5], it was hypothesised that lower temperatures would enable a better determination of the true path of the hot corrosion/stress mechanism proposed by Brooking et al. [17]. That is, was the path associated with the interface between the gamma prime and gamma, or within the gamma prime? Hence, a series of stress corrosion tests have been conducted on the Ni-base superalloys, CMSX-4, CM247LC DS and IN6203DS, at temperatures of 550, 500 and 450 °C.

Table 1 Chemistries (wt %) of superalloys obtained from material certificates

Superalloy	Ni	C	Cr	Co	W	Nb	Ta	Hf	Ti	Al	Re	Zr	Mo
CMSX-4	61.2	0.004	6.5	9.5	6.4	–	6.4	0.1	1.0	5.5	2.8	–	0.6
CM247LC DS	61.5	0.08	8.1	9.3	9.5	–	3.2	1.5	0.7	5.6	–	0.01	0.5
IN6203DS	48.8	0.16	21.4	18.7	2.0	0.8	1.1	1.1	3.5	2.3	–	0.06	< 0.1

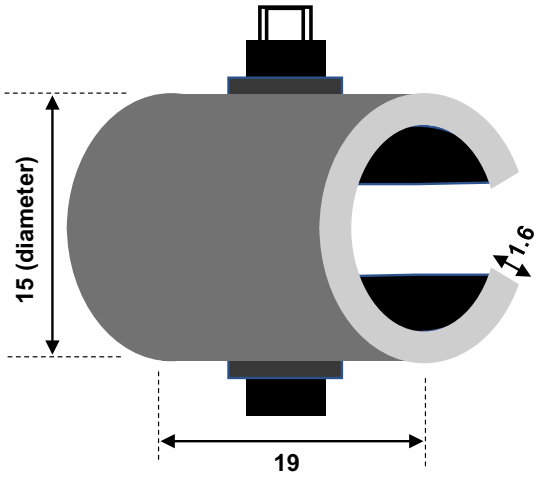

Fig. 1 Illustration of C-ring test specimen (dimensions shown in mm before stress is applied via the stainless steel bolt and nut)

Materials and Methods

Materials and Test Specimen

The CMSX-4, CM247LC DS and IN6203DS Ni-base superalloys were supplied in the precipitation hardened state in the form of 5/8" diameter × 9" long bars that had been cast in the < 001 > orientation. Table 1 shows the chemistries of each superalloy which were obtained from the respective material certificates. The quoted values were originally obtained using the X-ray fluorescence method except for C (which was obtained using LECO analysis) and Ni which has been derived by arithmetic calculations.

The bars were subsequently machined into C-rings (Fig. 1) using low stress grinding technique.

Stress Corrosion Tests

The C-rings were cleaned using isopropyl alcohol in an ultrasonic tank. After drying, stainless steel (A2 grade) M5 nuts, bolts and washers were used to apply a stress in accordance with BS EN ISO 7539-5:1995 [18]—see Theory/calculation

section. The use of the A2 grade stainless steel nuts, bolts and washers was based on repeating the methodology of similar tests performed by Brooking et al. [17]. Once stressed, the C-rings were then subjected to hot corrosion exposures in a horizontal tube furnace using the deposit recoat practise [19]. The deposits used were a 4/1 molar ratio of Na_2SO_4/K_2SO_4, applied every 100 h, and the mass of these deposits was measured per unit area to achieve a nominal surface loading of 500 µg cm^{-2} on the outer surface of the C-rings. The temperatures at which the hot corrosion exposure was conducted at were 550, 500 and 450 °C (± 5 °C) in a gaseous environment of 300 ppm SO_2 in air which was vented through bubblers using NaOH as a scrubber.

At each interval of 100 h, a visual examination of the C-ring surfaces was performed to check for surface cracks. If cracking was observed, the respective C-ring was removed from any further exposures. If cracks were not observed, the C-rings were recoated with the deposits, and further exposure conducted. This was repeated up to a maximum test duration of 1000 h.

Sectioning and Preparation of Test Specimens

On completion of the hot corrosion exposures, the C-rings were subjected to a preliminary visual examination of the surfaces before sectioning as illustrated in Fig. 2. The subsequent micro-sections were polished to a one micron finish and examined in the as polished and etched states. Two electrolytic etchants were used during the examination using solutions of 40 ml of glycerol, 20 ml of hydrofluoric acid and 340 ml of water (which preferentially etched the gamma prime), and 1% of citric acid, 1% of ammonium sulphate and water (which preferentially etched the gamma). Between each etched state examination though, the respective specimen was re-polished to a one micron finish.

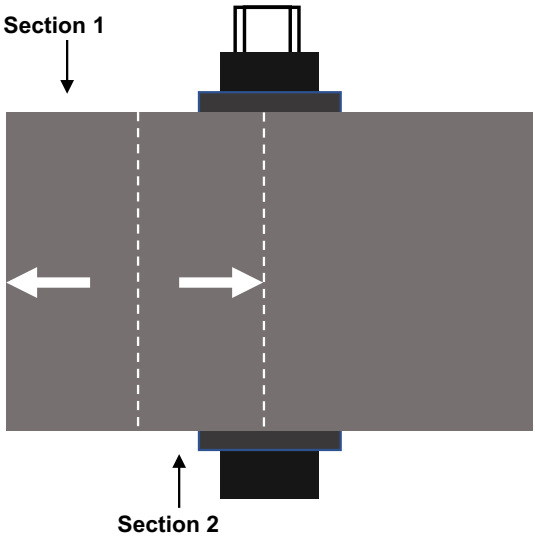

Fig. 2 Illustration of micro-sections from the C-rings. Arrows indicate the faces that were polished and examined

The half of the C-ring that was not sectioned was placed in a vice and tightened until a forced overload occurred. This forced overload would have occurred in areas that had reduced cross sections caused by the cracking and enabled examination of the resulting opened crack faces.

Microscopy Techniques

An Olympus GX51 optical microscope and a Jeol JSM-6460 scanning electron microscope (SEM) were used to conduct the preliminary visual examination to identify potential cracks on the surfaces of the C-rings. These techniques were repeated on the polished/etched micro-sections to identify any feature which may be associated with the potential cracks.

Characterisation of the hot corrosion products was performed using energy dispersive X-ray (EDX) mapping, with an accelerating voltage of 20 kV, and Inca software. This technique though, is unable to differentiate between Mo and S owing to overlapping X-ray energy peaks. However, due to the relatively small Mo content within the chemistries of the materials (Table 1) plus the S content within the deposits sprayed onto the C-ring surfaces, any Mo/S indication was assumed to be S.

Image analysis, using Olympus stream motion software, was performed on etched virgin materials for the purpose of assessing the gamma prime size and volume fraction.

Theory/Calculation

BS EN ISO 7539-5:1995 [18] provides equations for calculating a final diameter of the C-ring to give a desired maximum stress. These equations are:

$$D_f = D \pm \Delta D \tag{2}$$

$$\Delta D = \sigma \pi d^2 / 4EtZ \tag{3}$$

where

D_f = the outside diameter of the stressed C-ring measured at right angles to a centre line passing through the point of maximum stress (mm)
D = outside diameter of the C-ring before stressing (mm)
ΔD = the change of D to give the desired stress (mm)
σ = the desired stress within the limit of proportionality (MN/m^2)
d = the mean diameter (mm)
E = modulus of elasticity (MN/m^2)
t = wall thickness of the C-ring (mm)

Z = correction factor

The respective values of the various parameters are not given in this paper in order to protect the modulus of elasticity provided by Siemens Industrial Turbomachinery Limited.

Results and Discussion

A summary of all the C-ring testing performed is shown in Table 2 along with the result of whether cracking had occurred or not. These results were based on the observations gathered from the preliminary visual examinations, micro-sections, and the forced overload sections. The IN6203DS material showed no evidence of surface cracking after 1000 h of exposure at 550 °C, whilst CMSX-4 and CM247LC DS experienced cracking (Figs. 3 and 4) at all the test temperatures after a specific period of exposure. For CMSX-4, this specific period was 100 h irrespective of the test temperature. The first signs of cracking in CM247LC DS though were observed after 400 h at 550 °C and 200 h at both 500 and 450 °C. The shorter specific period of exposure at the lower temperatures for cracks to appear in CM247LC DS may be explained by the relaxation of the stainless steel bolts during the tests. Calculations based on the change in C-ring diameter before and after each period of 100 h of testing, indicated greater losses of applied stress for higher temperatures (Fig. 5). A similar loss of applied stress also occurred on IN6203DS during each period of 100 h of testing. It was assumed that the stainless steel bolts used for stressing the CMSX-4 C-rings had also relaxed. However, in this case, accurate measurements

Table 2 C-ring tests and results

Superalloy	Nominal stress (MPa)	Temperature (°C)			Duration (h)	Cracked?
		550	500	450		
CMSX-4	700	2 off			100	Yes
CMSX-4	700		2 off		100	Yes
CMSX-4	700			2 off	100	Yes
CM247LC DS	800	1 off			100	No
CM247LC DS	800	1 off			200	No
CM247LC DS	800	1 off			300	No
CM247LC DS	800	1 off			400	Yes
CM247LC DS	800	2 off			500	Yes
CM247LC DS	800		1 off		100	No
CM247LC DS	800		1 off		200	Yes
CM247LC DS	800		7 off		300	Yes
CM247LC DS	800			1 off	100	No
CM247LC DS	800			2 off	200	Yes
IN6203DS	800	2 off			1000	No

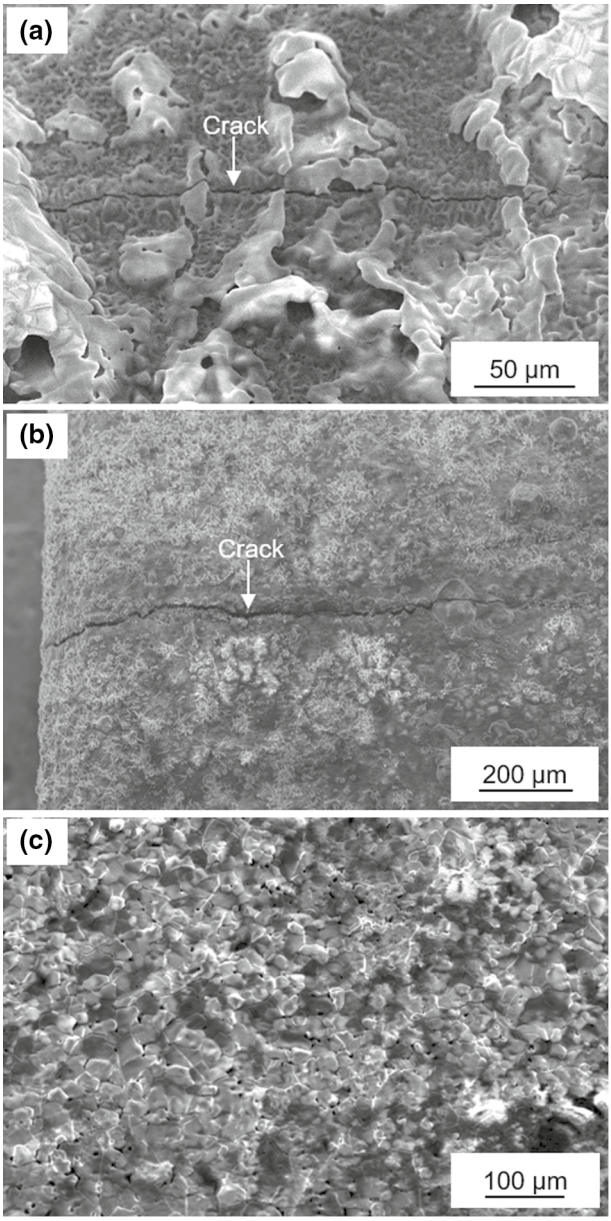

Fig. 3 Secondary electron images showing examples of surface cracking found on **a** CMSX-4 after 100 h at 500 °C and **b** CM247LC DS after 400 h at 550 °C. No evidence of surface cracking could be found on **c** IN6203DS after 1000 h at 550 °C

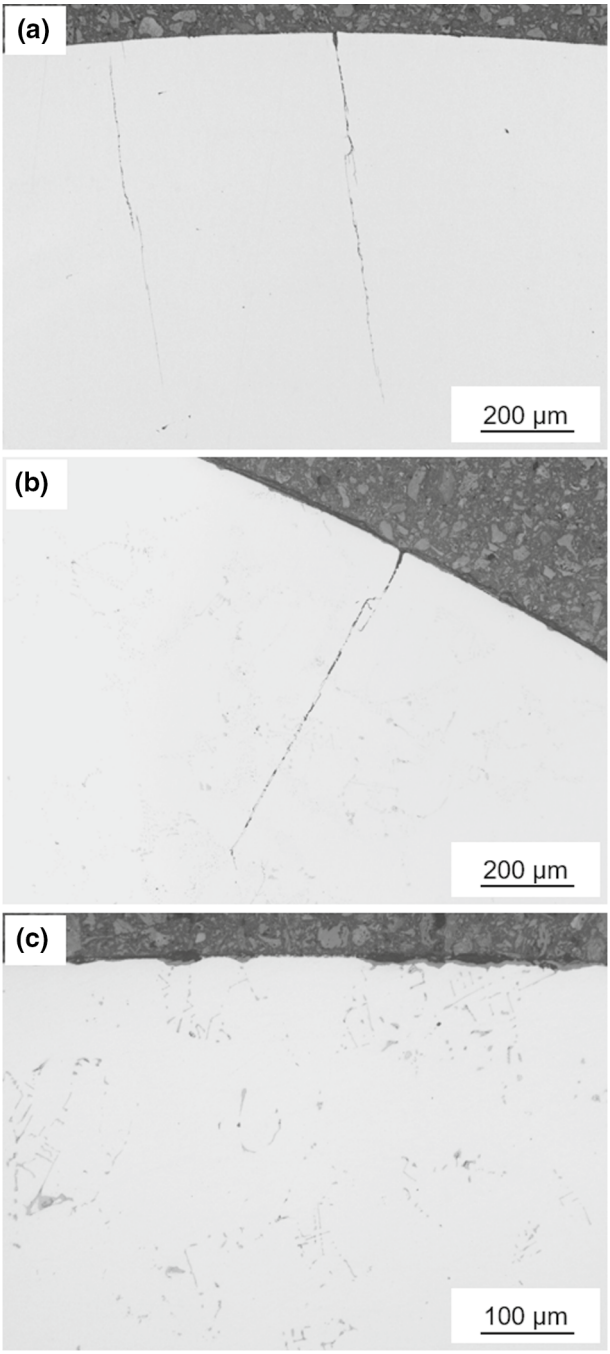

Fig. 4 Optical microscope images showing examples of cracking found in the unetched micro-sections of **a** CMSX-4 after 100 h at 550 °C and **b** CM247LC DS after 400 h at 550 °C. No evidence of cracking could be found in **c** IN6203DS after 1000 h at 550 °C

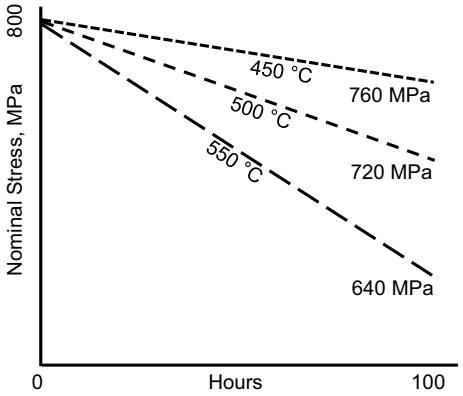

Fig. 5 Illustration showing the approximate change in the stress applied to CM247LC DS superalloy during each 100 h period of testing due to the relaxation in the stainless steel bolt

of the diameters in a stressed state after exposure could not be obtained as each CMSX-4 C-ring had cracked during the first period of testing. The stresses applied to the C-rings may therefore only be considered a nominal stress and not the true str ess.

A comparison of the CMSX-4 and CM247LC DS forced overload sections from the first C-rings to show signs of cracking (Fig. 6) indicated similarities in that

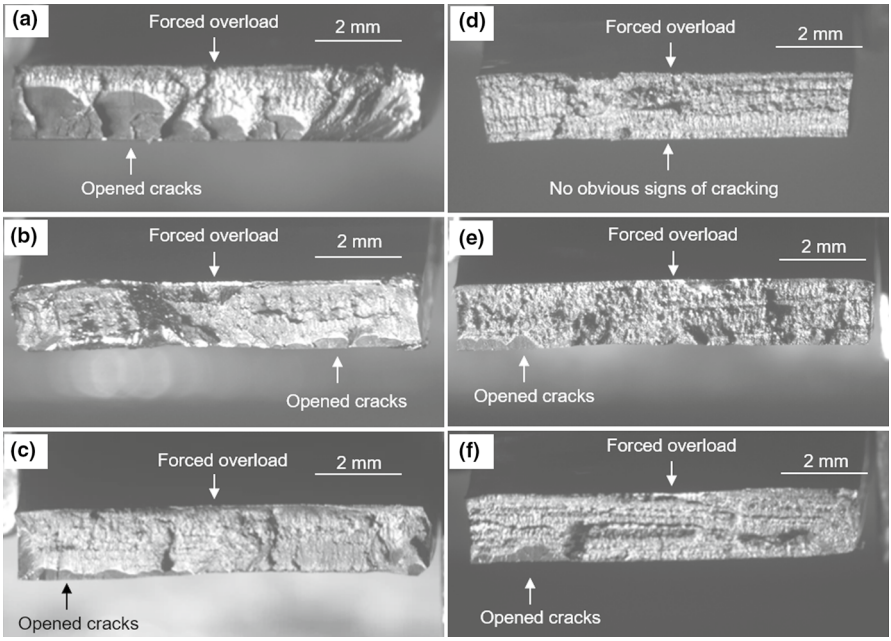

Fig. 6 Optical microscope images of forced overload sections of CMSX-4 C-rings **a**, **b** and **c** after 100 h exposure at 550, 500 for and 450 °C, respectively, and CM247LC DS C-rings **d**, **e** and **f** after exposure at 550 °C for 400 h, 500 °C for 200 h and 450 °C for 200 h, respectively

multiple cracking had generally occurred and the crack faces were roughly semi-circular in shape. The exception to this appears to be the CM247LC DS C-ring exposed at 550 °C for 400 h, Fig. 6d, which despite the evidence shown in Fig. 3b, appeared to show no obvious signs of cracking. However, SEM analysis did confirm very small semi-circular features (Fig. 7) which were consistent with cracking and suggested that, in the forced overload section, the crack initiation process was in the very early stages. Further, SEM analysis of the obvious opened crack faces from the other CMSX-4 and CM247LC DS forced overload sections revealed flow lines suggesting a sequence of multiple origins and in the case of CMSX-4, beach marks (Fig. 8). These indicated the cracks had propagated in a start-stop-start manner.

Examination of the etched micro-sections revealed the cracks in the CMSX-4 and CM247LC DS C-rings tended to propagate approximately normal to the direction of stressing and were associated with fingers of stress corrosion attack. The example shown in Fig. 9, CMSX-4 exposed at 550 °C for 100 h, was first etched using the hydrofluoric etchant which etches the gamma prime. This etchant clearly shows the stress corrosion had attacked the gamma prime and propagated in the orientation of the gamma prime. However, the etchant does tend to etch out the stress corrosion product leading to a possible false conclusion that the voids produced at the tip of the feature may be micro-cracks. After re-polishing and re-etching using the citric acid, which etches the gamma, the stress corrosion product was observed to be intact. Further to this, since temperature affects the diffusion rates, the C-rings exposed at the lower temperatures provided a clearer indication of the true path of the stress corrosion finger, and this was predominantly through the gamma prime rather than at the interface with the gamma (Fig. 10). Other fingers of stress corrosion attack though did not appear to have cracked. This is suggestive that the stress corrosion fingers, which looked to have a ‘wedge’ shape (Fig. 11), occurred before cracking. EDX mapping of the fingers (Figs. 12 and 13) confirmed the stress

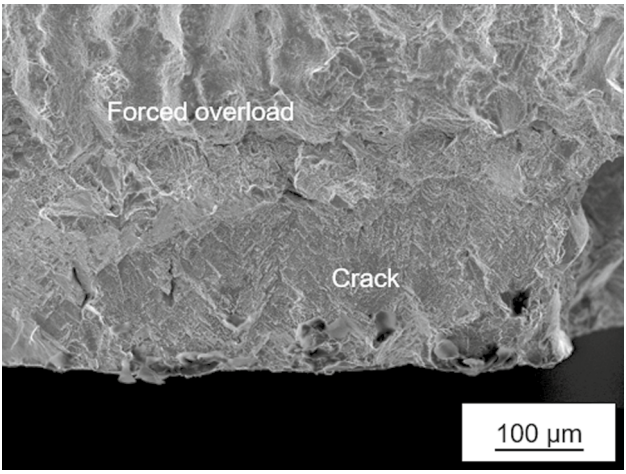

Fig. 7 Secondary electron image of forced overload section from CM247LC DS C-ring exposed at 550 °C for 400 h showing semi-circular crack feature

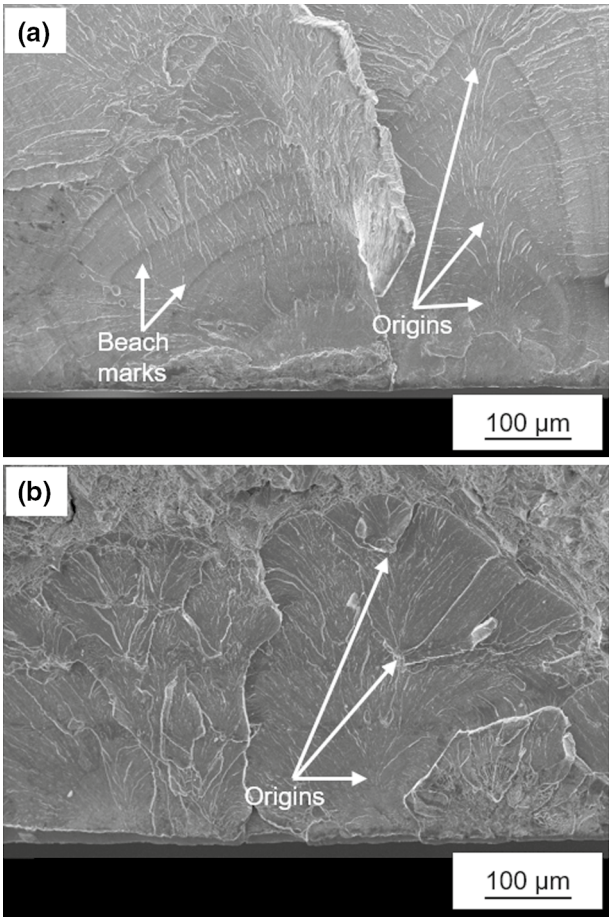

Fig. 8 Secondary electron images of opened crack faces within the forced overload sections from **a** CMSX-4 exposed at 550 °C for 100 h and **b** CM247LC DS exposed at 450 °C for 200 h

corrosion product was a similar compound for both the CMSX-4 and CM247LC DS materials and consisted of O_2, Al, Cr, Co, Ni, Na, S and K. Hence, the stress corrosion fingers were an O_2 and S embrittled phase.

The first C-rings to show signs of crack/stress corrosion fingers had the maximum depth of these features measured from the micro-sections (Table 3). Based on the exposure duration to the first signs of the cracks/fingers, it appears that CMSX-4 was more susceptible to the exposure conditions than CM247LC DS. The relationship between the micro-sections and the fingers was a random one though, and therefore, the observed depths are most likely not the true depths.

Since the gamma prime was susceptible to the stress corrosion attack, image analysis was performed on three random areas of CMSX-4, CM247LC DS and IN6203DS materials in the virgin condition (examples shown in Fig. 14). This was to provide gamma prime size and volume fraction data (Table 4), that could be

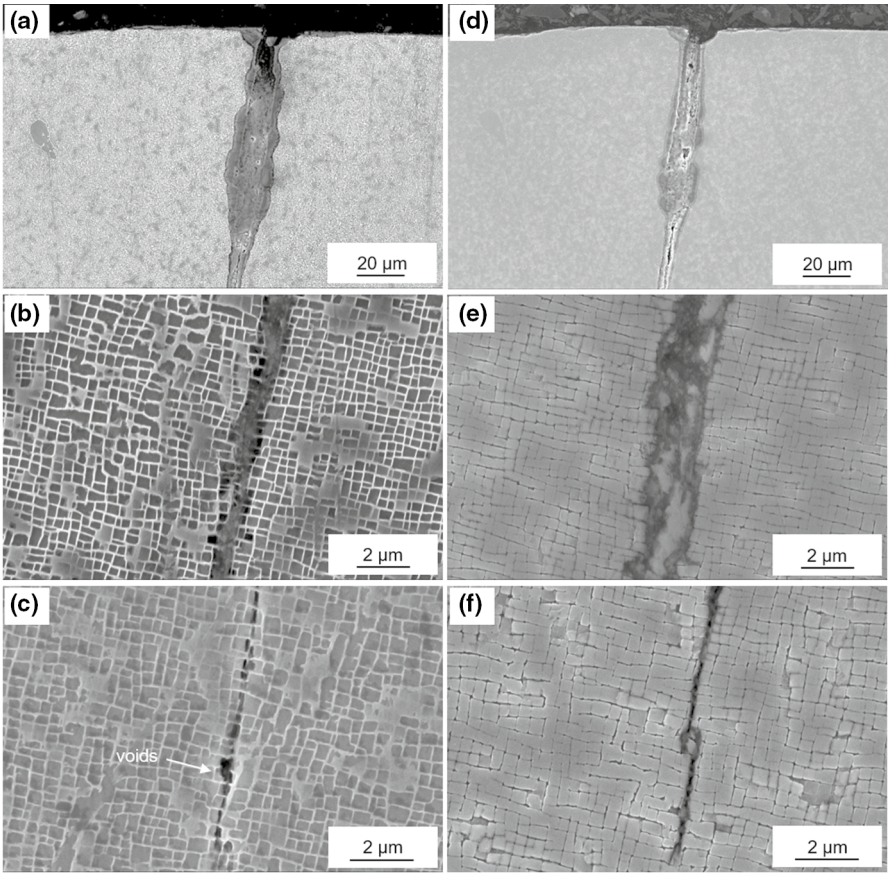

Fig. 9 Secondary electron images showing an example of a crack/stress corrosion finger observed in CMSX-4 C-ring exposed at 550 °C for 100 h. Images **a**, **b** and **c** show the start, mid and tip of the feature after etching in the hydrofluoric acid. Images **d**, **e** and **f** show the approximate same positions after re-etching in the citric acid

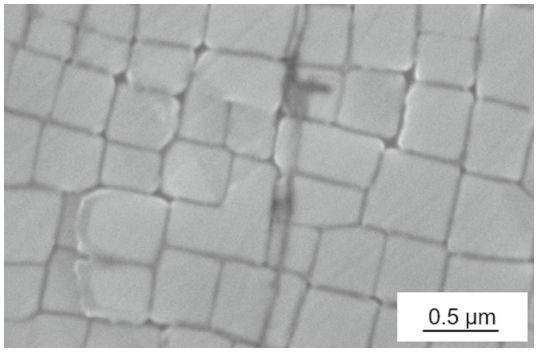

Fig. 10 Secondary electron image of CMSX-4 exposed at 450 °C for 100 h and etched in citric acid showing stress corrosion product propagating predominantly through the gamma prime near the tip of the feature

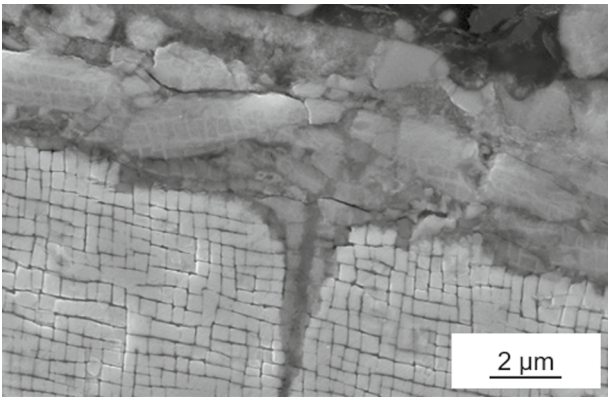

Fig. 11 Secondary electron image of a citric acid etched non-cracked wedge-shaped stress corrosion finger in CMSX-4 after exposure at 450 °C for 100 h

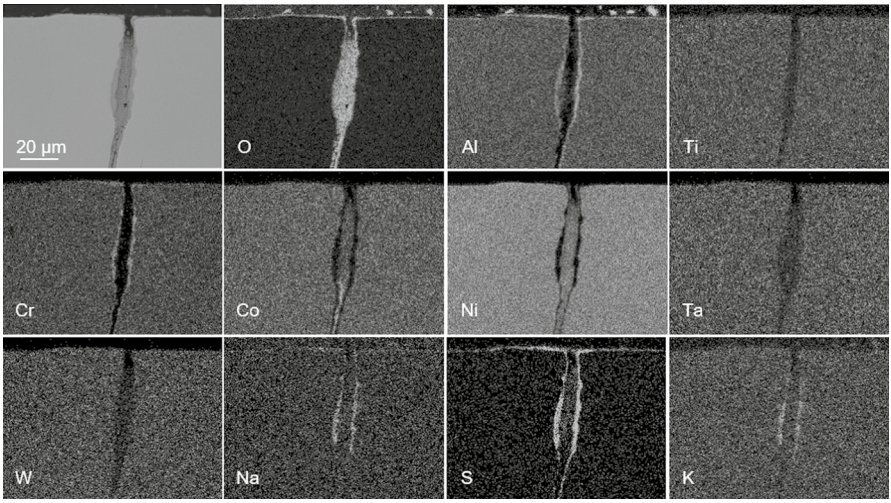

Fig. 12 EDX map of stress corrosion product in CMSX-4 exposed at 550 °C for 100 h

influenced by the respective chemistries of the superalloys, and subsequently used for correlation purposes with the stress corrosion cracking each material had experienced. After ranking the materials, with respect to the severity of cracking each had experienced, in the order of CMSX-4, CM247LC DS and finally IN6203DS, it was found that a correlation existed with the gamma prime volume fraction (rather than size) with averaged values of 60, 52 and 27%, respectively. These results indicated that when compared with CMSX-4, a gamma prime volume fraction reduction of 8% increased the resistance of CM247LC DS to the stress corrosion conditions in that it took longer for the first signs of cracking to appear at all of the test temperatures. A gamma prime volume fraction reduction of 33% though, appeared to have provided

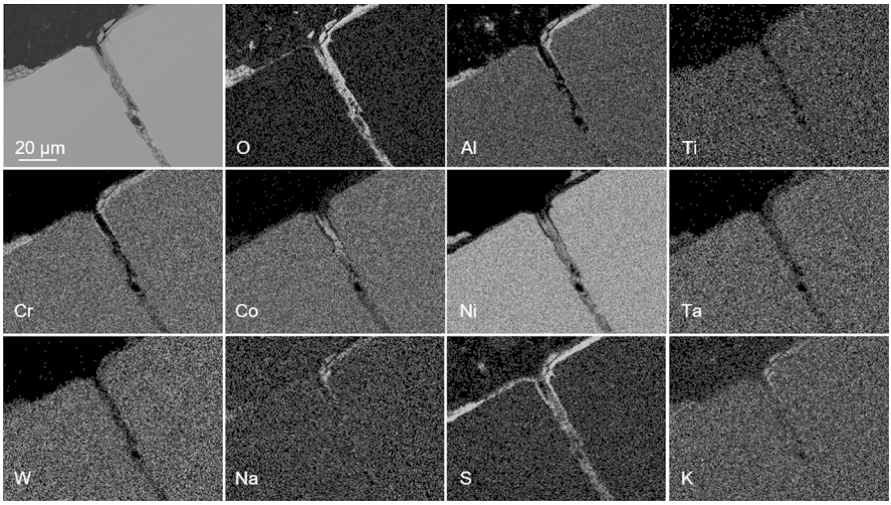

Fig. 13 EDX map of stress corrosion product in CM247LC DS exposed at 550 °C for 400 h

Table 3 Crack/stress corrosion finger depths

Superalloy	Test conditions			Maximum observed crack/stress corrosion depth (µm)
	Nominal stress (MPa)	Temp. (°C)	Duration (h)	
CMSX-4	700	550	100	840
CMSX-4	700	500	100	360
CMSX-4	700	450	100	230
CM247LC DS	800	550	400	805
CM247LC DS	800	500	200	443
CM247LC DS	800	450	200	455

immunity to the same conditions for IN6203DS with no signs of cracking at all at the highest test temperature of 550 °C. These improvements in the resistance to the stress corrosion conditions were achieved despite CM247LC DS and IN6203DS being tested with a nominal stress of 800 MPa as opposed to the 700 MPa used for CMSX-4. It is acknowledged though that the results of this assessment are based on an extremely limited data set.

It has been observed that the stress corrosion fingers of attack are associated with the gamma prime, either at the interface with the gamma, or more predominantly within the gamma prime (Fig. 10). These areas experience a summation of stresses which include the applied stress plus the mismatch stresses at the interface between the gamma prime and gamma, and those associated with the interstitial S atoms distorting the lattice structure within the gamma prime. This is suggestive that stress may accelerate the fingers of attack, providing the orientation of the gamma prime is

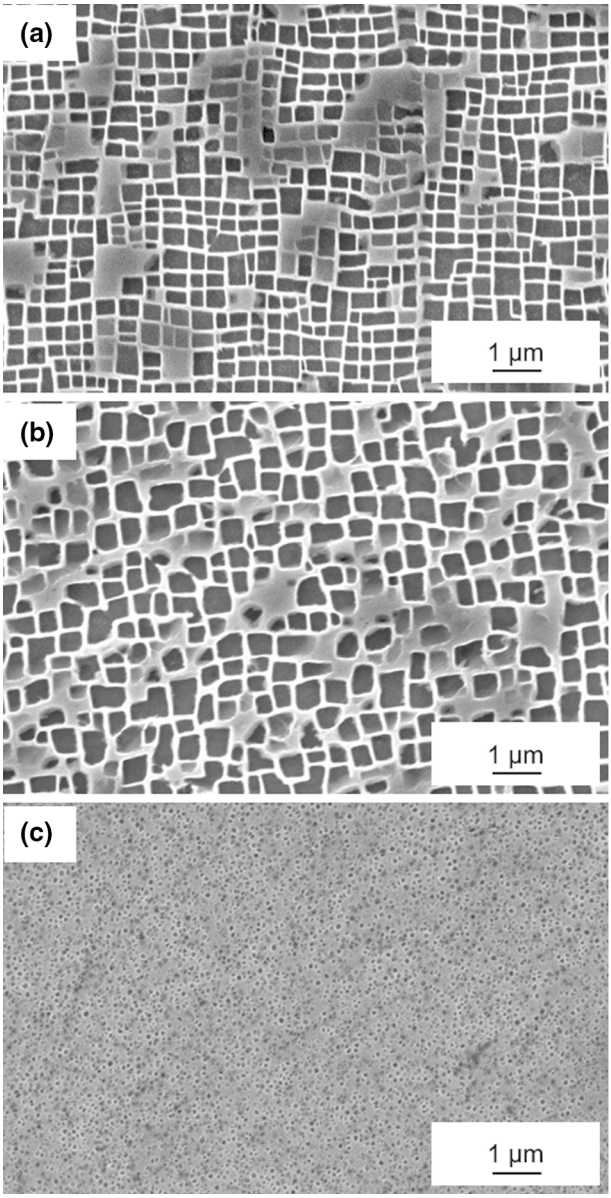

Fig. 14 Secondary electron images of examples of random areas of hydrofluoric etched virgin material showing gamma prime in **a** CMSX-4, **b** CM247LC DS and **c** IN6203DS

normal to the applied stress, and has led to a hypothesised crack mechanism which is illustrated in Fig. 15. In (a), corrosive species diffuse into the materials from the deposits on the surface to produce a scale shown in (b). In (c), the scale is accelerated normally to the applied stress in areas influenced by additional stresses. This

Table 4 Gamma prime data averaged from three random areas per superalloy

Superalloy	Ranking according to severity of cracking	Gamma prime size (mean feret, μm)	Gamma prime volume fraction (%)
CMSX-4	1	0.39	60
CM247LC DS	2	0.46	52
IN6203DS	3	0.12	27

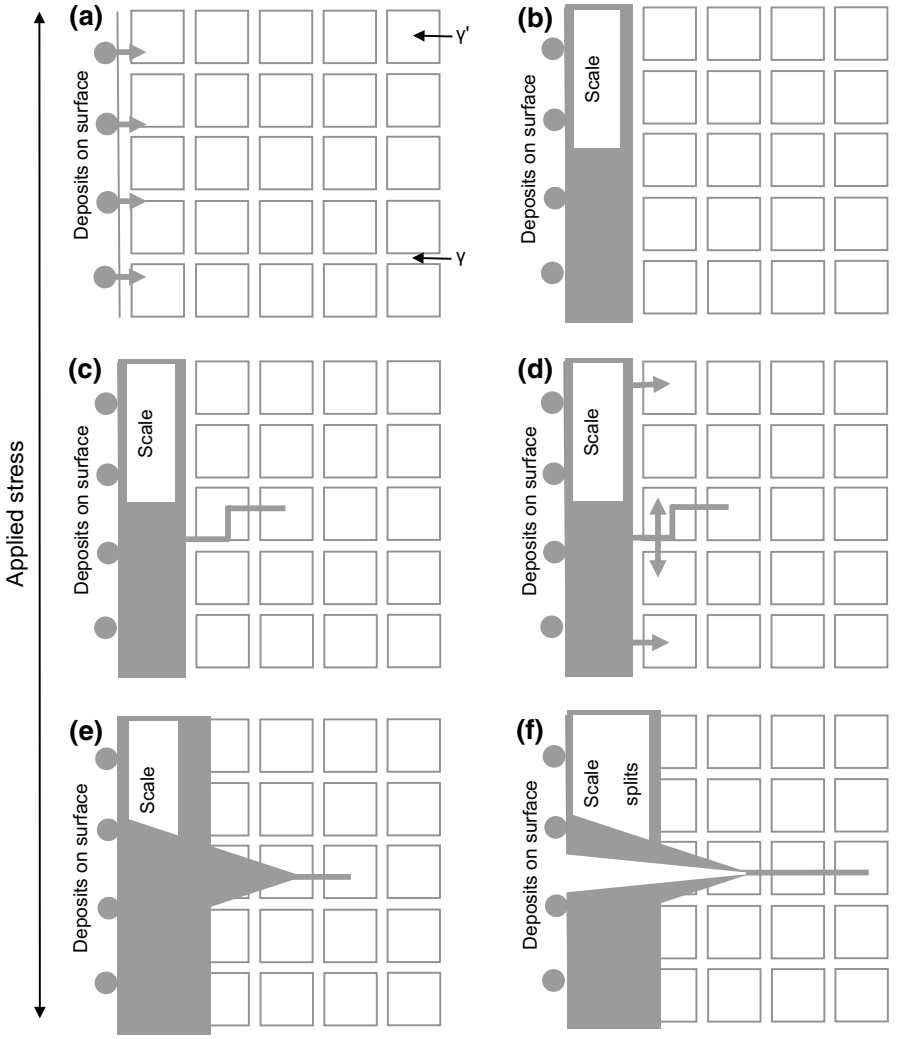

Fig. 15 Illustration showing the various stages of the proposed crack mechanism

may be due to stress raisers on the surface, such as scratches or pitting, which could be further exacerbated by the mismatch at the interface between the gamma prime and the gamma, and/or the interstitial S atoms that have diffused into the gamma prime distorting the lattice. The corrosive species would continue to diffuse in from the surface but would now also diffuse in the direction of the applied stress from the localised fingers (d) producing a wedge shape to the attack. This wedge would also act as a stress raiser and further accelerate the stress corrosion finger (e) normally to the applied stress. These fingers of attack would experience an embrittlement that allow the summation of stresses to split the scale (f) creating another stress raiser, countering the reduction in stress associated with the stress gradient across the C-ring. This would then ensure the stress corrosion finger continues to propagate and thereby repeat the process.

This hypothesised crack mechanism would explain the multiple surface cracking observed (Fig. 6)—any stress raiser on the surface (such as scratch, pit or any surface roughening) could initiate localised stress corrosion fingers. It would also accommodate the beach marks, flow lines and multiple origins within each crack (Fig. 8) since these features are consistent with the start-stop-start process insinuated by the proposed mechanism.

Conclusions

After completion of this research, the following conclusions were made:

- After exposure to the hot corrosion conditions at each of the test temperatures (550, 500 and 450 °C), both CMSX-4 and CM247LC DS materials experienced stress corrosion cracking whilst being subjected to nominal stresses of 700 and 800 MPa, respectively. The IN6203DS material though, which was only exposed at 550 °C and nominally stressed to 800 MPa, appeared to be immune to stress corrosion.
- The stress corrosion cracking which had occurred in CMSX-4 and CM247LC DS showed similar features including multiple surface cracks. After opening, the cracks revealed beach marks (on CMSX-4 only), flow lines and sequences of origins suggesting the cracks propagated in a start-stop-start manner. Microsections also revealed that the cracks were associated with localised fingers of stress corrosion attack containing compounds consisting of O_2, Al, Cr, Co, Ni, Na, S and K. These fingers tended to propagate through the gamma prime when the orientation of the precipitates coincided with being approximately normal to the applied stresses. No localised finger of stress corrosion attack was observed when the orientation of the precipitates was not approximately normal to the applied stresses.
- The gamma prime volume fraction, which may be influenced by the Cr and Co levels within the respective superalloys, appeared to be correlated to the severity of stress corrosion cracking experienced with CMSX-4 showing the worst severity, followed by CM247LC DS and then IN6203DS. This suggests lower gamma prime volume fractions increase the resistance to stress corrosion cracking and

infers that Ni-base superalloys possessing inherently good creep properties may be susceptible to stress corrosion cracking.

- A stress corrosion cracking mechanism was proposed which suggested the summation of stresses experienced accelerated the stress corrosion attack of the gamma prime when the orientation of the gamma prime was approximately normal to the applied stress. The summation of stresses includes the applied stress, surface stress raisers, the mismatch stresses at the interface between the gamma prime and the gamma, and distortional stresses associated with the interstitial S atoms. Variations in the total stress experienced would therefore produce multiple localised stress corrosion fingers which are an embrittled phase that eventually split. The split then acts as another stress raiser and continues to drive the fingers of attack ensuring the process is repeated in a start-stop-start manner.

Acknowledgements The authors would like to thank Siemens Industrial Turbomachinery Limited for funding this work.

Authors' Contributions All authors contributed to the conception and design of the study. Material preparation, experimental work, data collection/analysis and imaging were performed by Neil Chapman. The first draft of the manuscript was written by Neil Chapman. All authors commented on previous versions of the manuscript. All authors read and approved the final manuscript.

Funding This research has been funded by Siemens Industrial Turbomachinery Limited.

Availability of Data and Material The data cannot be shared at this time as it is part of an ongoing study.

Compliance with Ethical Standards

Conflict of interest The authors declare that they have no conflict of interest.

Code Availability Not applicable.

Open Access This article is licensed under a Creative Commons Attribution 4.0 International License, which permits use, sharing, adaptation, distribution and reproduction in any medium or format, as long as you give appropriate credit to the original author(s) and the source, provide a link to the Creative Commons licence, and indicate if changes were made. The images or other third party material in this article are included in the article's Creative Commons licence, unless indicated otherwise in a credit line to the material. If material is not included in the article's Creative Commons licence and your intended use is not permitted by statutory regulation or exceeds the permitted use, you will need to obtain permission directly from the copyright holder. To view a copy of this licence, visit http://creativecommons.org/licenses/by/4.0/.

References

1. P. Caron and T. Khan, *Aerospace Science and Technology* **3**, 1999 (513). https://doi.org/10.1016/S1270-9638(99)00108-X.
2. N. El-Bagoury, *International Journal of Engineering Sciences and Research Technology* **5**, 2016 (108).

3. G. Brunetti, A. Settefrati, A. Hazotte, S. Denis, J. J. Fundenberger, A. Tidu and E. Bouzy, *Micron* **43**, 2012 (396). https://doi.org/10.1016/j.micron.2011.10.009.
4. F. Pyczak, B. Devrient and H. Mughrabi, *Superalloys* **2004**, 2004 (827). https://doi.org/10.7449/2004/superalloys_2004_827_836.
5. R. C. Reed, *The Superalloys Fundamentals and Applications*, (Cambridge University Press, Cambridge, 2006).
6. H. Mughrabi, *Acta Materialia* **81**, 2014 (21). https://doi.org/10.1016/j.actamat.2014.08.005.
7. R. D. Field, T. M. Pollock, and W. H. Murphy, *Superalloys* 557 (1992).
8. H. Lai, *High Temperature Oxidation and Corrosion of Ni-Based Superalloys for Industrial Gas Turbines* [PhD thesis] (Chalmers University of Technology, Goteborg, 2014).
9. B. Bourdenet, *High Temperature Corrosion in Gas Turbines: Thermodynamic Modelling and Experimental Results* [PhD thesis] (RWTH Aachen University, Saarbrucken, 2004).
10. N. Birks, G. H. Meier and F. S. Pettit, *Journal of the Minerals, Metals and Materials Society* **39**, 1987 (28). https://doi.org/10.1007/BF03257568.
11. J. Sumner, A. Encinas-Oropesa, N. J. Simms and J. R. Nicholls, *Oxidation of Metals* **80**, 2013 (553). https://doi.org/10.1007/s11085-013-9395-x.
12. F. Pettit, *Oxidation of Metals* **76**, 2011 (1). https://doi.org/10.1007/s11085-011-9254-6.
13. W. J. Zhang and R. Sharghi-Moshtaghin, *Metallurgical and Materials Transactions A* **49**, 2018 (4363). https://doi.org/10.1007/s11661-018-4755-4.
14. J. M. Alvarado-Orozco, J. E. Garcia-Herrera, B. Gleeson, F. S. Pettit and G. H. Meier, *Oxidation of Metals* **90**, 2018 (527). https://doi.org/10.1007/s11085-018-9853-6.
15. E. Kistler, W. T. Chen, G. H. Meier and B. Gleeson, *Materials and Corrosion* **70**, 2019 (1346). https://doi.org/10.1002/maco.201810751.
16. K. Chen, L. R. Zhao and J. S. Tse, *Acta Materialia* **51**, 2003 (1079). https://doi.org/10.1016/S1359-6454(02)00512-8.
17. L. Brooking, J. Sumner, S. Gray and N. J. Simms, *Materials at High Temperatures* **35**, 2018 (120). https://doi.org/10.1080/09603409.2017.1392414.
18. Corrosion of metals and alloys—part 5: preparation and use of C-ring specimens, BS EN ISO 7539-5:1995.
19. J. Sumner, A. Encinas-Oropesa, N. J. Simms and J. R. Nicholls, *Materials and Corrosion* **65**, 2014 (188). https://doi.org/10.1002/maco.201307425.

Publisher's Note Springer Nature remains neutral with regard to jurisdictional claims in published maps and institutional affiliations.

https://dspace.org/

Stress corrosion testing of CMSX-4, CM247LC DS and IN6203DS Ni-base superalloys

Chapman, Neil; Gray, Simon; Sumner, Joy; Nicholls, John R.

2020-11-23
Springer
https://doi.org/10.1007/s11085-020-10011-w
Chapman N, Gray S, Sumner J, Nicholls J. (2021) Stress corrosion testing of CMSX-4, CM247LC DS and IN6203DS Ni-base superalloys. Oxidation of Metals, Volume 95, Issue 1-2, February 2021, pp. 85-104

Downloaded from a DSpace repository. https://dspace.org/